

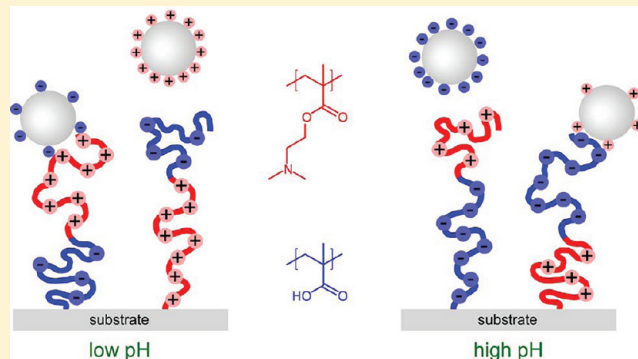
## Formation of Polyampholyte Brushes via Controlled Radical Polymerization and Their Assembly in Solution

Young K. Jhon,<sup>†,‡</sup> Shafi Arifuzzaman,<sup>†,§</sup> Ali E. Özçam,<sup>†,||</sup> Douglas J. Kiserow,<sup>†,‡</sup> and Jan Genzer<sup>\*†</sup>

<sup>†</sup>Department of Chemical and Biomolecular Engineering, North Carolina State University, Raleigh, North Carolina 27695-7905, United States

<sup>‡</sup>Army Research Office, Research Triangle Park, North Carolina 27709-2211, United States

**ABSTRACT:** We describe the formation of polyampholytic block copolymer brushes and their assembly in solution. Specifically, we employ “surface-initiated” activators regenerated by electron transfer atom transfer radical polymerization (ARGET-ATRP) sequentially to form diblock copolymer grafts comprising blocks of poly[2-(dimethylamino)ethyl methacrylate] (PDMAEMA) and poly(sodium methacrylate) (PNaMA) on flat impenetrable silica surfaces, i.e.,  $\text{SiO}_x/\text{PNaMA}-b\text{-PDMAEMA}$  and  $\text{SiO}_x/\text{PDMAEMA}-b\text{-PNaMA}$ . Protonation of the PNaMA block results in formation of poly(methacrylic acid) (PMAA). We demonstrate that ARGET-ATRP of NaMA provides a convenient route to preparation of PMAA, which is an alternative method to the more traditional approach based on preparing PMAA by polymerizing *tert*-butyl methacrylate (tBMA) followed by cleavage of the *tert*-butyl group. We also discuss conformational changes of the individual polyelectrolyte blocks in solution as a function of solution pH by monitoring adsorption behavior of functionalized polystyrene spheres.



### 1. INTRODUCTION

Due to their unprecedented ability to functionalize surfaces with chemical tailoring and responsive properties, surface-anchored brushes have been employed in generating ‘smart’ responsive materials.<sup>1–6</sup> While most of the initial work involved preparation of homopolymer brushes, recent efforts have turned toward application of polymeric grafts bearing multiple chemical moieties.<sup>7,8</sup> To that end, the behavior of grafted macromolecular assemblies involving various chemical functionalities has been explored that involve both neutral as well as chargeable groups.<sup>9</sup> Initial efforts have revealed that polyampholyte brushes may represent a convenient platform and a burgeoning area of research because of their unprecedented tailorability resulting in unique behavior on surfaces.<sup>10–15</sup>

Polyampholytes are macromolecules that bear both positive and negative charges along their backbone; these charges are either permanent (strong or quenched polyelectrolytes) or can be induced by varying the pH of the solution (weak or annealed polyelectrolytes). The conformation of polyampholytes in solution thus depends on the relative amounts of the two charges and their distribution along the backbone. As in any polyelectrolyte system, the behavior of polyampholytes in solution is governed by a broad set of parameters, including the degree of polymerization of both blocks, the degree of dissociation (i.e., the number of charges) along each block, the concentration of external salt (i.e., the solution ionic strength), the interaction parameters between the polymer segments and solvent molecules, and the

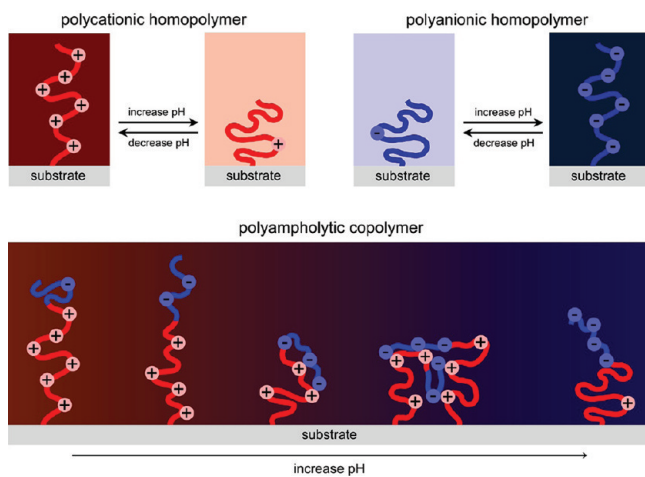
sequence distribution of the charged moieties along the macromolecule.<sup>16</sup> The behavior of polyampholytes with either net positive or net negative charges is governed by strong repulsion between like charged monomers, which tends to extend the chain and help to dissolve the chains even in relatively poor solvents for the backbone (i.e., the polyelectrolyte effect). The charge sequence in neutral polyampholytes is important. For example, polyampholytes with an alternating sequence of opposite charges are typically swollen, whereas polyampholytes consisting of block (or blocky) sequences may collapse and precipitate from solution.<sup>17–19</sup> While the bulk behavior of polyampholytes has been investigated for some time, studies of the interfacial behavior of polyampholytes are still in their infancy. This is primarily due to the difficulties associated with preparing such systems and also the large set of parameters to be explored. Nearly all interfacial studies on polyampholytes reported to date involve their adsorption on solid interfaces, while only a few studies have reported preparing polyampholyte brushes on surfaces and characterizing their properties.<sup>12,20–25</sup>

Figure 1 depicts a schematic representation of conformational changes of a polycationic homopolymer brush, a polyanionic homopolymer brush, and a polyampholytic brush comprising both polycationic and polyanionic blocks as a function of the

**Received:** September 21, 2011

**Revised:** November 22, 2011

**Published:** November 23, 2011



**Figure 1.** Illustrations of the suggested conformations of (A) polycationic homopolymer brushes, (B) polyanionic homopolymer brushes, and (C) polyampholytic copolymer brushes as a function of the solution pH.

solution pH. At low pH, the polycationic block is fully charged while there are only a few charges present in the polyanionic block. Due to repulsions among the positive charges along the polycationic block, the block copolymer assumes an extended conformation in solution. While the number of charges along the polycationic block decreases with increasing pH, there is a concurrent increase in the number of negative charges generated along the polyanionic block. Depending on the number of charged groups along the copolymer and their sequence, the presence of both charges will either cause the brush to stretch even farther away from the surface or decrease the brush thickness because the polymer chains may form a compact/collapsed structure,<sup>19</sup> with individual chains interacting, self-collapsing, or folding down on their neighbors due to attractive interactions between the positive charges on the polycationic chains and the negative charges on polyanionic chains, as shown in Figure 1. Finally, at higher pH, the number of charges along the polycationic block is reduced dramatically, while the upper polyanionic block becomes almost completely charged, which leads to an increase in brush length.

Atom transfer radical polymerization (ATRP) offers a convenient means of synthesizing end- and body-functionalized polymers, including polyampholytes, with well-defined composition and relatively low polydispersities in molecular weight.<sup>26–28</sup> Although ATRP is remarkably tolerant to many functional groups, in practice, acrylic acid and methacrylic acid cannot be polymerized directly with currently available ATRP catalysts because these monomers interact with the metal complexes to form metal carboxylates that are inefficient deactivators and cannot be reduced to activate ATRP.<sup>28,29</sup> A typical approach is to employ the ATRP of *tert*-butyl acrylate (tBA) or *tert*-butyl methacrylate (tBMA),<sup>30,31</sup> initiated either in bulk or on the surface (i.e., “grafting from”), followed by hydrolysis or pyrolysis of the *tert*-butyl ester protective groups.<sup>32–37</sup> The polymerization rate for sterically hindered monomers such as *tert*-butyl methacrylate may be quite slow, as observed by Haddleton and co-workers.<sup>33</sup> Moreover, acid hydrolysis may result in cleavage of polymer chains from the surface.<sup>32,36,38</sup> An alternative method for preparing poly(methacrylic acid) (PMAA) brush without using methacrylic acid (MAA) involves polymerization of sodium

methacrylate (NaMA). Billingham, Armes, and co-workers first reported on ATRP of NaMA in aqueous media.<sup>39</sup> Osborne et al. employed a modified version of their procedure to grow polyelectrolyte brushes from gold-coated silicon surfaces.<sup>22</sup> A detailed report on the surface polymerization kinetics and the influence of temperature, pH, monomer concentration, and ionic strength on NaMA ATRP was presented by Tugulu et al.<sup>40</sup> Ober and co-workers reported on the room-temperature ATRP of the same monomer;<sup>41</sup> they also provided a detailed analysis of the dissociation behavior of polyelectrolyte brushes created using this method.<sup>42</sup>

In spite of all the advantages ATRP offers, there are several disadvantages that limit its widespread use. Successful ATRP, i.e., control over chain length and polydispersity, depends on highly active transition-metal/ligand catalyst systems. Therefore, special handling procedures are required to remove all oxygen and oxidants from the system. Another major difficulty is associated with the use of high catalyst concentrations as the transition-metal complexes must be removed from the reaction mixture and recycled, which increases production costs.<sup>43</sup> Although a number of techniques have been developed to reduce the residual transition metal in the final product, including, adsorption, extraction, and immobilization,<sup>43–50</sup> the most convenient method may simply be to decrease the amount of catalyst used in the reaction.<sup>51</sup>

In this study, we describe an alternative synthetic methodology for growing PMAA brushes on silica substrate by circumventing the limitations associated with PMAA synthesis from hydrolysis of tBMA. We illustrate that PMAA brushes can be synthesized by first polymerizing NaMA via activators regenerated by electron transfer atom transfer radical polymerization (ARGET-ATRP)<sup>51–53</sup> and protonating the resultant PNAMA. By combining the ARGET-ATRP of PNAMA with polymerization of 2-(dimethylamino)ethyl methacrylate (DMAEMA) we create ampholytic block copolymer brushes with either sequence of the two blocks on silica surfaces, i.e., SiO<sub>x</sub>/PMAA-*b*-PDMAEMA and SiO<sub>x</sub>/PDMAEMA-*b*-PMAA. In this paper we describe the procedures leading to formation of such polyampholytic assemblies and provide insight into conformational changes due to solution pH by monitoring the partitioning of amine- and carboxylate-terminated polystyrene latex particles.

## 2. EXPERIMENTAL SECTION

**2.1. Materials and Supplies.** The polymerization initiator used in this work was (11-(2-bromo-2-methyl)propionyloxy)undecyl-trichlorosilane, Br(CH<sub>3</sub>)<sub>2</sub>CCOO(CH<sub>2</sub>)<sub>11</sub>SiCl<sub>3</sub> (BMPUS); it was synthesized following a two-step procedure described by Matyjaszewski and co-workers.<sup>35</sup> N,N,N',N'',N'''-Pentamethyldiethylenetriamine (PMDETA), copper(II) chloride (CuCl<sub>2</sub>), methanol, anhydrous toluene, 2,2'-bipyridine (BiPy), L-ascorbic acid (AA), sodium methacrylate (NaMA), and 2-(dimethylamino)ethyl methacrylate (DMAEMA) were all purchased from Aldrich. Aqueous suspensions of carboxylate-modified polystyrene latex beads (yellow-green, 1 μm in diameter, Aldrich) and aqueous suspensions of amine-modified polystyrene latex beads (yellow-green, 1 μm in diameter, Aldrich) were used as received. Silicon wafers [100; 1–5 Ω·cm] were supplied by Silicon Valley Microelectronics, Inc.

**2.2. Formation of Polyampholyte Brushes Using ARGET-ATRP.** Silicon wafers were cut into 1 × 3 cm<sup>2</sup> pieces and subjected to ultraviolet/ozone treatment for 15 min in order to generate a large number of surface-bound hydroxyl groups. The surfaces of the silicon wafers were covered with the BMPUS polymerization initiator following

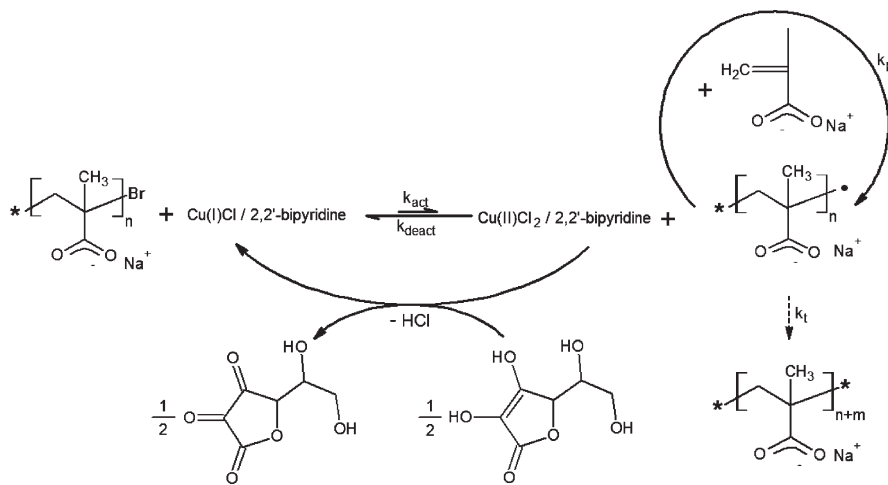


**Figure 2.** Reaction mechanism for ARGET-ATRP of NaMA.

the protocol described elsewhere<sup>54</sup> and subsequently rinsed with anhydrous toluene in order to remove any physically absorbed BMPUS molecules. Poly(sodium methacrylate) (PNaMA) brushes and poly-[2-(dimethylamino)ethyl methacrylate] (PDMAEMA) brushes were grown via a “grafting from” method from the substrate-bound BMPUS centers following the ARGET-ATRP mechanism. For the polymerization of NaMA, BMPUS-functionalized silicon wafer was incubated in NaMA aqueous solution (3.3 M NaMA, 1.9 mM CuCl<sub>2</sub>, 3.8 mM BiPy, 1.0 mM AA, and 49.3 mM methanol) for various times (5–60 min) at room temperature (25 °C). Initially, NaMA was dissolved in deionized (DI) water at pH 9 and the pH of the resulting solution was adjusted using HCl according to the optimization procedure described by Tugulu et al. for ATRP of this monomer.<sup>40</sup> For example, a 10 min polymerization of NaMA resulted in an 18.6 nm PNaMA dry brush thickness on the substrate. The monomer solution, an appropriate amount of CuCl<sub>2</sub>/BiPy, and AA solution were mixed in a 100 mL jar inside the dipper chamber without degassing or purging; a constant flow of nitrogen was maintained throughout the polymerization reaction. After polymerization of NaMA, the substrate was kept in deionized water with pH 1 for 12 h and then washed with methanol and deionized water to generate PMAA brushes.<sup>55</sup> For the polymerization of DMAEMA, a BMPUS-functionalized silicon wafer was kept in DMAEMA aqueous solution (6.6 M DMAEMA, 3.7 mM CuCl<sub>2</sub>, 7.5 mM BiPy, 2.8 mM AA, and 96.0 mM methanol) for various times. For example, a 4 h polymerization of DMAEMA resulted in 19.5 nm PDMAEMA dry brush thickness on the silicon wafer. There were two configurations for creating a tethered diblock polyelectrolyte brush: (1) a bottom PMAA anionic block and a top PDMAEMA block (i.e., SiO<sub>x</sub>/PMAA-*b*-PDMAEMA) and (2) a bottom cationic PDMAEMA block and a top PMAA block (i.e., SiO<sub>x</sub>/PDMAEMA-*b*-PMAA). Finally, the substrate was kept in a pH 1 solution for 12 h and washed with methanol and deionized water to convert PNaMA into PMAA.<sup>55,56</sup>

**2.3. UV-visible (UV-vis) Spectroscopy.** UV-vis spectroscopy was performed using a Varian Cary 100 spectrophotometer equipped with a dual-beam chamber, where sample solutions containing various molar ratios of AA and CuCl<sub>2</sub> were measured. Initial stock solutions for this measurement consisted of 2 mM CuCl<sub>2</sub> and 4 mM BiPy in DI water and methanol mixture without AA aqueous solution. Each measurement was carried out within a few seconds after solution preparation as a function of increasing AA/CuCl<sub>2</sub> mole ratio using a cuvette containing 1 mL of fresh solution. All absorbance intensities were collected in the range 350–900 nm with increments of 10 nm.

**2.4. Ellipsometry.** The thicknesses of PDMAEMA, PNaMA, PMAA, and polyampholytes brushes were measured at various points

on the silicon wafer using variable angle spectroscopic ellipsometry (VASE; J.A. Woollam, Inc.). The dry thickness was evaluated from the experimentally measured ellipsometric angles  $\Psi$  and  $\Delta$  collected from 400 to 1100 nm using 10 nm steps and a 70° angle between the direction of the beam and the sample normal using the commercial software provided by J. A. Woollam (WVASE32). A three-layer Cauchy model for Si/SiO<sub>x</sub>/homopolymer (either PDMAEMA, PNaMA, or PMAA) was employed to evaluate the index of refraction of the homopolymer films. The top layer thickness of the polyampholyte brushes was characterized using a four-layer Cauchy model. The following refractive indices were used for this measurement: 1.45 for BMPUS, 1.517 for PDMAEMA, 1.48 for PMAA, and 1.401 for PNaMA at 633 nm.<sup>25,57</sup>

**2.5. X-ray Photoelectron Spectroscopy (XPS).** The surface chemical compositions of PNaMA and PMAA samples were determined using Kratos Axis Ultra DLD XPS and monochromatic Al K $\alpha$  radiation with charge neutralization. Survey and high-resolution spectra were collected with pass energies of 80 and 20 eV, respectively, using both electrostatic and magnetic lenses at a takeoff angle of 90° for single-angle spectra collection. Atomic concentrations of selected elements were determined from the XPS spectral analysis using VISION and CasaXPS software packages.

**2.6. Contact Angle Analysis (CA).** The static contact-angle (sessile drop technique) experiments were performed with DI water (Resistance  $\approx$  18 MΩ·cm), aqueous solutions with pH 2 and pH 10 using a Ramé-Hart contact-angle goniometer (model 100-00) equipped with a CCD camera, and analyzed with the Ramé-Hart Imaging 2001 software. The advancing contact angles were recorded by injecting 6  $\mu$ L of the probing liquid on the specimen surface; the receding contact angles were determined after contacting the liquid drop with the probing needle. Contact angles were measured on at least five independent spots on each sample, and the average values were reported with corresponding standard errors.

**2.7. Adsorption of Functionalized Polystyrene Beads Using Fluorescence Microscopy.** Two types of aqueous suspensions of fluorescently labeled amine- and carboxylate-terminated polystyrene beads (1  $\mu$ m in diameter) were prepared as dilute solutions (0.25% w/w) with pH 2.5, 5.5, 7.0, and 10.0. One drop from each solution was applied to each substrate, i.e., SiO<sub>x</sub>/PDMAEMA and SiO<sub>x</sub>/PMAA homopolymers and SiO<sub>x</sub>/PMAA-*b*-PDMAEMA and SiO<sub>x</sub>/PDMAEMA-*b*-PMAA copolymers. After 10 min of exposure, all surfaces were washed copiously with DI water with corresponding pH values of the aqueous suspensions and then blow dried using nitrogen gas to remove any moisture. The coverage of fluorescent polystyrene beads on the surface was characterized using a medium-magnification (10 $\times$ )

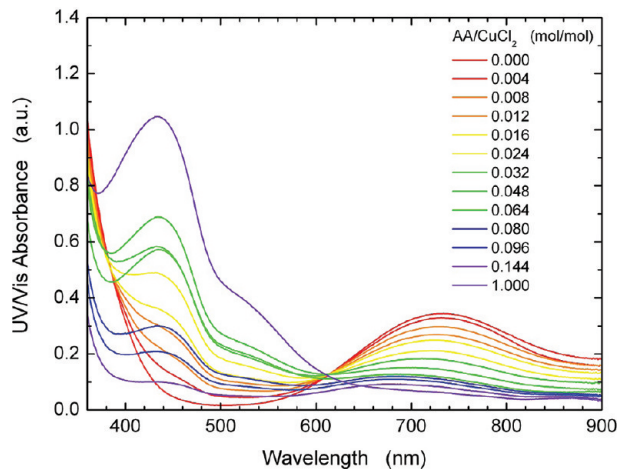


**Figure 3.** UV-vis absorbance as a function of wavelength from solutions of ascorbic (AA) and CuCl<sub>2</sub> in water and methanol mixture as a function of the AA/CuCl<sub>2</sub> ratio.

Olympus BX-61 optical microscope equipped with a fluorescence-mode FITC filter. The images were recorded using an Olympus DP-70 digital CCD camera.

### 3. RESULTS AND DISCUSSION

**3.1. Effect of the Amount of Reducing Agent on the Growth Rate of PNaMA via ARGET-ATRP.** Atom transfer radical polymerization (ATRP) involves a repetitive atom transfer process and functions by establishing an equilibrium between a dormant macromolecular alkyl halide and a redox-active transition-metal complex Cu(I)–X/Ligand. Matyjaszewski and co-workers devised a new method for conducting ATRP, so-called activators regenerated by electron transfer atom transfer radical polymerization (ARGET-ATRP), and demonstrated that this methodology enables controlled polymerization with a significant reduction of the amount of copper-based complex through the constant regeneration of the Cu(I) activator by a reducing agent.<sup>51</sup> The reducing agent, ascorbic acid (AA), enables ATRP with oxidatively stable Cu(II), lowers the catalyst concentration significantly (to parts per million levels with respect to the monomer), and tolerates a limited amount of oxygen or other radical traps in the system (cf. Figure 2). Therefore, the chemical reaction can be carried out without any deoxygenation or use of a vacuum or Schlenk line,<sup>58</sup> thus greatly simplifying the polymerization process.

Although previous work reported that the control of ARGET-ATRP is unaffected by excess reducing agent,<sup>58</sup> appropriate selection of the reducing agent and its concentration are crucial. For instance, the reducing agent will be consumed quickly if the initial concentration is kept low; the rate of polymerization would be very slow. In contrast, a large excess of the reducing agent may lead to fast and uncontrolled polymerization or unwanted side reaction with the catalyst. Since ATRP is a catalytic process, the appropriate amount of the catalyst is among the most important parameters to be established for these reactions. In order to gain insight into the reduction of Cu(II) by AA, we performed UV-vis measurements on different molar ratios of AA/Cu(II) solutions, with the results shown in Figure 3. The spectrum of CuCl<sub>2</sub>/BiPy/AA in water and methanol exhibits two characteristic

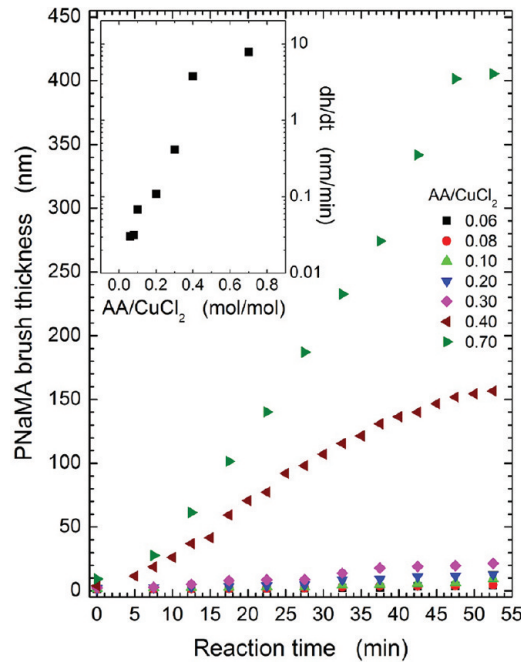


**Figure 4.** Dry thickness of poly(sodium methacrylate) (PNaMA) brushes as a function of reaction time for various ratios of ascorbic (AA) and CuCl<sub>2</sub>. (Inset) Rate of polymerization defined as the initial slope in the dry thickness ( $h$ ) vs time ( $t$ ) plot as a function of the AA/CuCl<sub>2</sub> ratio.

maxima in the spectral region 350–900 nm. The absorption peaks around 430 and 730 nm are attributed to an AA to Cu(II)–halide charge-transfer transition and the d–d bond of Cu(II)–halide, respectively.<sup>59–61</sup> Overall, the UV-vis data confirm the reduction of CuCl<sub>2</sub>/BiPy to CuCl/BiPy by AA and provide an indirect measurement of the relative concentrations of both species in the reaction mixture.

In order to study the time dependence of the AA/CuCl<sub>2</sub> ratio, we “projected” the ARGET-ATRP reaction onto a substrate by immersing a silicon wafer coated with the BMPUS initiator with constant rate into the polymerization solution containing the same amount of monomer and solvent and a variable amount of AA/CuCl<sub>2</sub>. We used this “dipping” method earlier to monitor the polymerization kinetics in “surface-initiated” ATRP.<sup>62</sup> By knowing the dipping rate, the position coordinate on the substrate can be converted conveniently into polymerization time. The data in Figure 4 depict the time dependence of the dry thickness of dry PNaMA, as measured by variable-angle spectroscopic ellipsometry (VASE). The data in the inset demonstrate that the chain growth rate increases with increasing the amount of AA in the reaction vessel. As the concentration of the metal complex activator, Cu(I)/Ligand, increases with increasing amount of reducing agent, homolytic cleavage of the alkyl halide bond,  $P_n-X$ , generates reversibly an alkyl radical,  $P_n^\bullet$ , and the corresponding higher oxidation state metal halide deactivator Cu(II)–X/Ligand (cf. Figure 2). The growing radicals propagate with a vinyl monomer (M) that can be deactivated by Cu(II)–X/Ligand or terminated by either coupling or disproportionation with another radical  $P_n^\bullet$ , at which point two equivalents of deactivator accumulate. The equation of the polymerization rate shown in eq 1 demonstrates that the polymerization rate depends only on the Cu(II)/Cu(I)

ratio and does not depend on the absolute concentration of the copper complexes.<sup>27,53</sup>

$$R_p = k_p[M][P_n \cdot] = k_p[M]K_{ATRP}[P_n - X] \frac{[\text{Cu(I)}/\text{Ligand}]}{[\text{Cu(II)}/\text{Ligand}]} \quad (1)$$

where  $K_{ATRP}$  is the ratio of  $k_{act}$  to  $k_{deact}$ .

The intensity of UV-vis absorption at 730 nm from Figure 3 and the polymerization rate from Figure 4, which is defined here as the initial slope of dry thickness ( $h$ ) with reaction time ( $t$ ), are plotted in Figure 5 as a function of the AA/CuCl<sub>2</sub> ratio. The data in Figure 5 reveal that at lower molar ratio of AA the

polymerization rate (circles) is very low and remains nearly constant, yet there is a strong reduction in the mole ratio of Cu(II) (squares). Only after reaching a certain molar ratio of AA the polymerization rate increases dramatically with increasing the AA/CuCl<sub>2</sub> ratio. This behavior is consistent with the prediction of eq 1, i.e., increasing the molar ratio of AA that leads to greater reduction of the ATRP deactivator Cu(II) and concurrent production of the ATRP activator Cu(I), which results in an ultimately higher Cu(I)/Cu(II) ratio and a higher polymer growth rate. However, the behavior at a small molar ratio of AA/CuCl<sub>2</sub> is quite complex, because AA is also involved in scavenging excess oxygen present in the system in addition to reducing Cu(II) to Cu(I).

### 3.2. Formation and Properties of Polyampholyte Diblock Copolymer Brushes.

Polyampholyte brushes were formed by sequential ARGET-ATRP of two monomers. First, the bottom block was grown from the substrate-grafted BMPUS polymerization centers. This was followed by polymerization of the second block from the substrate-bound macroinitiator. The dry thicknesses of both blocks of the polyampholyte brushes are plotted in Figure 6 for both combinations of blocks considered. The data demonstrate clearly that tethered diblock polyelectrolyte brushes can be prepared that consist of either a cationic PDMAEMA bottom block and an anionic PNaMA top block (cf. Figure 6a) or an anionic PNaMA bottom block and a cationic PDMAEMA top block (cf. Figure 6b). The PDMAEMA brush was created on a BMPUS-covered silicon wafer with 19.5 nm (dry thickness), and then an 18.6 nm PNaMA brush was grown on the PDMAEMA brush. The top PNaMA block can be protonated, yielding PMAA without damaging the PDMAEMA layer as evidenced by the fact that the dry thickness of the bottom block did not change during protonation (cf. Figure 6a). In order to determine the robustness of this synthetic approach for preparing a diblock polymer brush with bottom PNaMA and top PDMAEMA blocks, we first grew a PNaMA brush on an initiator-covered silicon wafer, then used these PNaMA macroinitiator

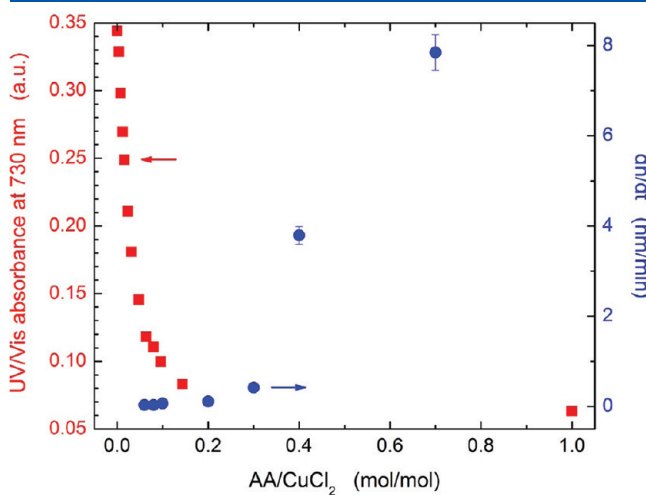


**Figure 5.** (Left ordinate, squares) UV-vis absorption intensity at 730 nm as a function of the AA/CuCl<sub>2</sub> ratio. (Right ordinate, circles) Rate of polymerization of sodium methacrylate (NaMAA) defined as the initial slope in the dry thickness ( $h$ ) versus time ( $t$ ) as a function of the AA/CuCl<sub>2</sub> ratio.

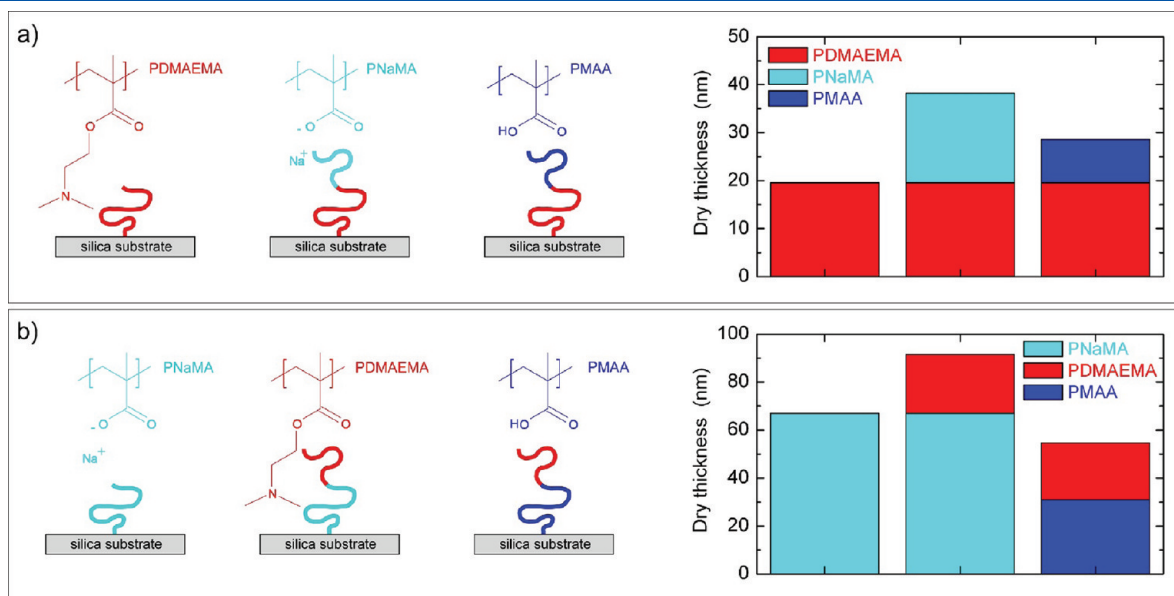


**Figure 6.** Illustrations and dry thickness of polyampholyte brushes prepared by (a) first growing poly[2-(dimethylamino)ethyl methacrylate] (PDMAEMA) block, followed by growth of poly(sodium methacrylate) (PNaMA) top block, and finally converting the top PNaMA block into poly(methacrylic acid) (PMAA) and (b) first growing PNaMA, followed by growth of PDMAEMA top block, and finally converting the bottom PNaMA block into PMAA.

brushes to grow the top PDMAEMA block, and finally PNaMA-*b*-PDMAEMA was converted to PMAA-*b*-PDMAEMA. Specifically, AA was added to the same DMAEMA solution that was prepared previously and the wafer with PNaMA macroinitiators ( $\sim 66.7$  nm in thickness) was kept in the polymerization solution for 3 h. This step resulted in a 24.6 nm PDMAEMA polymer brush on top of the PNaMA brush. Finally, the substrate with PNaMA-*b*-PDMAEMA brush was kept in a pH 1 solution for 12 h to protonate the PNaMA block and was washed with methanol and deionized water. The latter procedure resulted in the reduction of the thickness of the bottom block but did not affect the thickness

of the top PDMAEMA block, which clearly shows the robustness of the approach (cf. Figure 6b).

XPS experiments confirmed that the aforementioned conversion of PNaMA into PMAA took place, i.e., it removed all sodium (cf. Figure 7). The major component peaks in the C 1s (280–294 eV) region are representative of the mixture of C–C/C–H (285.0 eV), C–O/C–O–C (286.6 eV), O–C–O/C=O (287.9 eV), and O=C=O (289.0 eV) signals, and the peaks in O 1s (525–540 eV) are a combination of the C=O (532.8 eV) and C–O (533.6–544.3 eV) signals from the carbonyl group.<sup>63–65</sup> The major difference in the XPS signals before and after protonating PNaMA is indicated by the absence of sodium ion peaks, located at 1072.6, 64.0, and 31.0 eV, which correspond to the Na 1s, Na 2s, and Na 2p signals.<sup>65</sup>

Water contact-angle (WCA) measurements have been carried out on substrates grafted with both homopolymers and copolymers in order to test the response of the system to different pH values. Substrates decorated with pure PMAA exhibit a decrease in the WCA with increasing pH (cf. Figure 8). This behavior is expected as the polyanionic homopolymer becomes more hydrophilic when more negative charges, induced at higher pH, are present on the polymer backbone (cf. Figure 1). In contrast, the WCA measured on PDMAEMA brushes decreases with decreasing pH (cf. Figure 8). In the latter case, the PDMAEMA becomes charged at low pH (cf. Figure 1), which explains the lower WCA with decreasing pH of the probing solution. There is a difference in wettabilities of the homopolymer brushes with a single charge type. Specifically, at low pH the WCA of PMAA is lower than that of PDMAEMA at higher pH. This behavior can be attributed to better wettability of the PMAA chains relative to PDMAEMA (which contains more hydrophobic groups along the repeat unit). The wettability studies performed with polyampholytic macromolecular grafts reveal that the copolymers follow the same trends (and are virtually quantitatively the same) as the homopolymers, whose chemical composition is identical to the

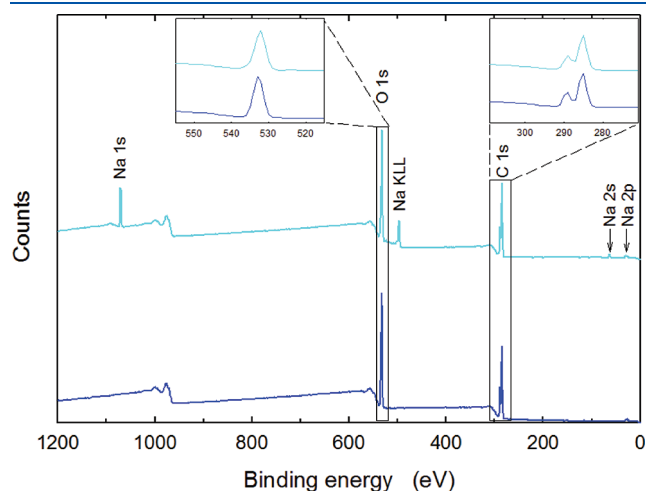


**Figure 7.** X-ray photoelectron spectroscopy (XPS) spectra from poly(sodium methacrylate) (PNaMA) (upper cyan line) and poly(methacrylic acid) (PMAA) (lower blue line) demonstrating quantitative conversion of PNaMA to PMAA. XPS spectra in the inset show no changes to carbon and oxygen peaks during the PNaMA to PMAA conversion.

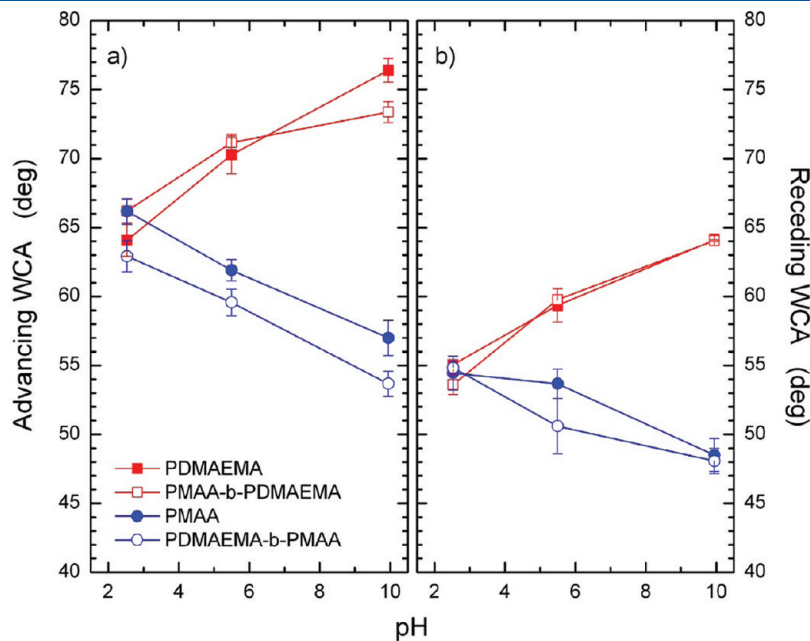


**Figure 8.** Advancing water contact angles (WCA; a, left ordinate) and receding water contact angles (WCA; b, right ordinate) of PDMAEMA, PDMAEMA-*b*-PMAA (i.e., top block PDMAEMA), PMAA, and PMAA-*b*-DMAEMA (i.e., top block PMAA) as a function of the pH of the probing aqueous solution.

top block of the copolymer. A small exception to the aforementioned trends is that the wettability of  $\text{SiO}_x/\text{PDMAEMA}$ -*b*-PMAA is slightly better than that of  $\text{SiO}_x/\text{PMAA}$ . We attribute

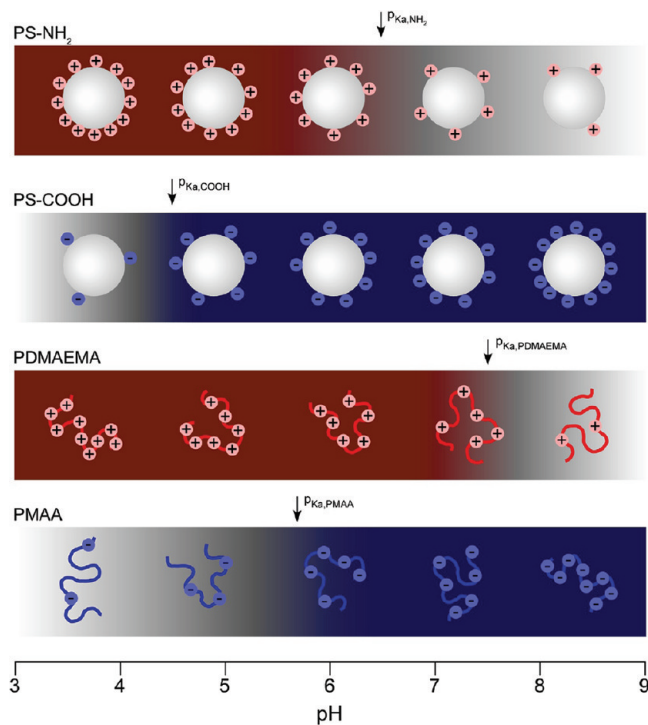


**Figure 9.** Illustration of the charge distribution in PMAA, PDMAEMA, and  $-\text{COOH}$ - and  $-\text{NH}_2$ -terminated PS latex spheres. Sizes of polymers and latex spheres are not drawn to size. The arrows represent  $pK_a$  values of each homopolymer brush and the surface functional groups on PS latex spheres.

the latter behavior to the presence of a hydrophobic BMPUS in the  $\text{SiO}_x/\text{PMAA}$  case, which may be “seen” by the probing liquid. The receding angles are nearly identical. Overall, the wettability results demonstrate the wettability cannot be employed to detect any conformational changes in the block copolymer polyampholyte structure because it probes changes in the topmost  $\sim 0.5$  nm thick layer of the brush where the topmost portion of the polymeric graft is sensed by the probing liquid.

### 3.3. Conformational Changes of Polyampholyte Blocks Due to pH Variation.

The WCA experiments described earlier confirmed the presence and function of the individual building blocks. However, only the top block in the polyampholytic diblock could be detected by WCA measurements due to extreme surface sensitivity of the method. In order to provide further insight into the conformational behavior of both blocks present in the polyampholyte brush as a function of pH, we employ fluorescently labeled polystyrene (PS) latex particles decorated with two types of ionic functional groups, i.e., primary amine (PS- $\text{NH}_2$ ) and carboxylate (PS- $\text{COOH}$ ). Due to the larger size of PS particles used in this study compared to the average distance between grafted polyampholyte chains, the PS latex beads could not penetrate the polyampholytes brushes; instead, they interact with the top surface of the brush. We expected the strong electrostatic interactions and hydrogen bonding between the functional groups on the PS latex particle surface and the respective blocks to overcome these conformational constraints. In order to regulate the charge density, these experiments were run in four different pH values: (i) pH 2.5, i.e., below the  $pK_a$  of PMAA ( $pK_{a,\text{PMAA}} = 5.7^{66}$ ) and PDMAEMA ( $pK_{a,\text{PDMAEMA}} = 7.5^{67}$ ); (ii) pH 5.5, i.e., close to the  $pK_{a,\text{PMAA}}$ ; (iii) pH 7.0, i.e., close to the  $pK_{a,\text{PDMAEMA}}$ ; and (iv) pH 10.0, i.e., above  $pK_{a,\text{PMAA}}$  and  $pK_{a,\text{PDMAEMA}}$ . We note that the cited  $pK_a$  values correspond to bulk properties of polymers and that they may differ when applied to surface-anchored polymers.<sup>68</sup>

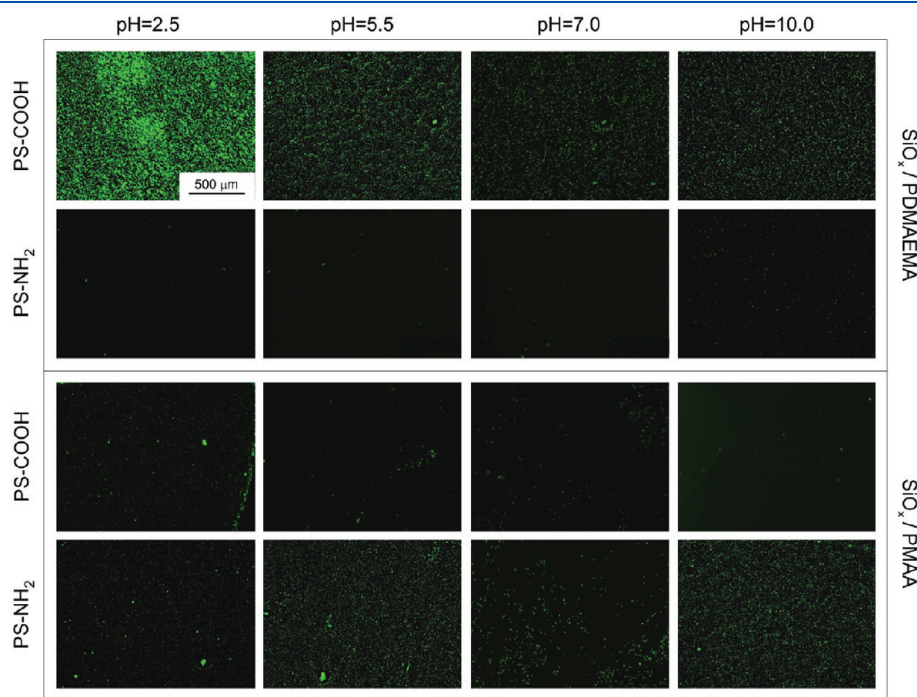


**Figure 10.** Fluorescence microscopy images depicting the adsorption of PS latex particles with  $-\text{COOH}$  and  $-\text{NH}_2$  termination on PDMAEMA brushes (top panel, dry thickness of PDMAEMA = 59 nm) and PMAA brushes (bottom panel, dry thickness of PMAA = 59 nm) as a function of pH.

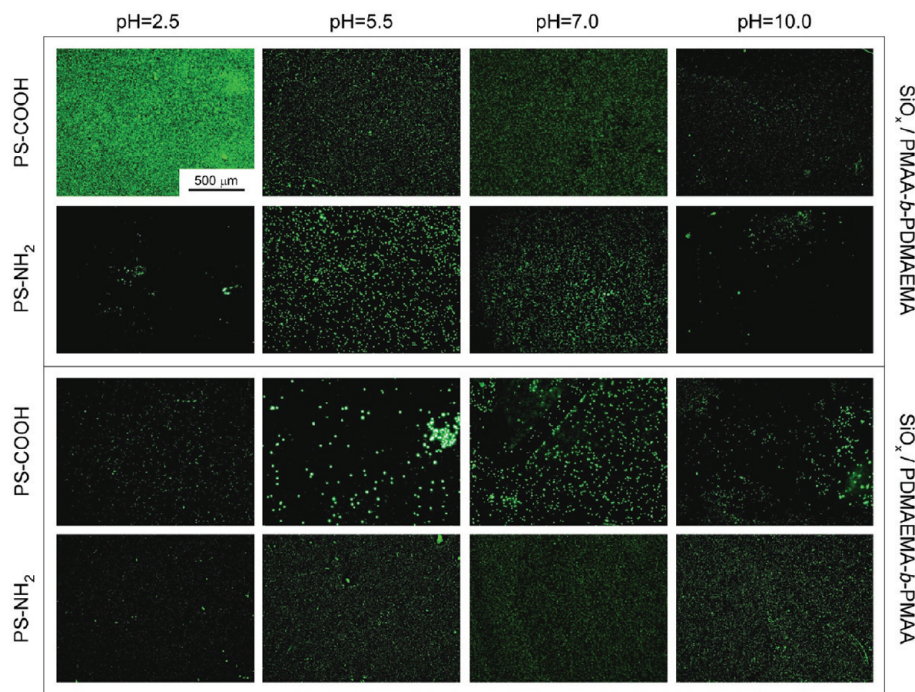


**Figure 11.** Fluorescence microscopy images depicting the adsorption of PS latex particles with  $-COOH$  and  $-NH_2$  termination on PDMAEMA-*b*-PMAA brushes (top panel, dry thickness of PDMAEMA = 142 nm and PMAA = 56 nm) and PMAA brushes (bottom panel, dry thickness of PMAA = 14 nm and PDMAEMA = 9 nm) as a function of pH.

In addition, we illustrate schematically the charge density of positive ions on a surface of an amine-modified PS bead (PS- $NH_2$ ), negative ions on a carboxylate-modified PS bead (PS- $COOH$ ), quaternized nitrogen atoms along a PDMAEMA brush, and carboxylated ions along a PMAA brush as a function of solution pH in Figure 9. The arrows in Figure 9 indicate the  $pK_a$  values of the  $-NH_2$  groups on PS particles,<sup>69,70</sup> the  $-COOH$  groups on PS particles,<sup>71,72</sup> the tertiary amines in PDMAEMA brushes, and the carboxylate groups in PMAA brushes. More than one-half of the amine groups are protonated below the  $pK_a$  values of primary amines on PS particles and tertiary amines PDMAEMA brushes. More than one-half of the carboxylate groups are deprotonated above the  $pK_a$  values of the carboxylate groups on PS particles and PMAA brushes, respectively. Adsorption of fluorescently dyed PS spheres (yellow-green) to homopolymer (cf. Figure 10) and polyampholyte (cf. Figure 11) brushes was monitored by fluorescence microscopy. No attempts were made to quantify the fluorescence intensity from the micrographs.

The adsorption of functionalized PS beads on charged brushes is governed by the balance of two phenomena: (1) interaction among PS particles in bulk solution and (2) interaction between the particles and the brushes. In addition to electrostatic interaction (either attractive or repulsive, depending on the charge) hydrogen bonding may also play a role in particle partitioning on the substrate. Because of a complex interplay among the various types of interactions and also the fact that the degree of charging inside the weak polyelectrolyte brush may be different from that of the bulk system<sup>68</sup> and is not well understood, understanding the observations may be challenging. We will proceed with discussing the partitioning of PS latex spheres on homopolymer brushes and use those results as benchmarks when discussing the adsorption of PS particles on top of polyampholytes.

In Figure 10 we present fluorescence micrographs depicting the adsorption of amino- and carboxylate-terminated PS spheres on top of PDMAEMA (top) and PMAA (bottom) brushes. Let us commence the discussion by considering adsorption of functional PS latex particles onto PDMAEMA brushes. At low pH PS- $COOH$  adsorbs on PDMAEMA brushes quite strongly (first row in Figure 10). This is likely due to both electrostatic interactions between the positively charged PDMAEMA and weakly negatively charged  $-COOH$  as well as hydrogen bonding between the particle and the brush. With increasing pH, the carboxy-terminated PS particles adsorb less strongly on PDMAEMA brushes because of strong charge–charge repulsion among negatively charged particles in solution and decreasing ionic interactions between the particles and brushes due to a decreasing number of positively charged PDMAEMA groups present in the brush. Because the primary and tertiary amine groups on PS- $NH_2$  and PDMAEMA are both charged positively at low pH and remain neutral at high pH, hydrogen bonding is the only likely type of interaction that allows the PS- $NH_2$  particles to interact with the underlying PDMAEMA brushes at relatively high pH, where interparticle repulsion in solution is small.<sup>73,74</sup> As the data in the second row in Figure 10 indicate, particle adsorption is quite small, revealing that the density of hydrogen bonds between primary and tertiary amines is not high enough. We now turn to the adsorption of the functional PS latex spheres onto PMAA brushes. Adsorption of PS- $COOH$  occurs primarily through hydrogen bonds at low pH, where both carboxyls on the particle and those in the brush remain neutral. With increasing pH the adsorption between the PS- $COOH$  particles and the PMAA brushes weakens because of interparticle repulsion in solution and particle/brush repulsion. The images presented in the third row in Figure 10 confirm this trend. The adsorption of PS- $NH_2$  particles on PMAA is quite complex (fourth row in Figure 10).

At low pH, the interparticle repulsion dominates and only a small number of particles are allowed to approach the substrate. With increasing pH, the charge density on the particles decreases while that on the brush increases, leading to a larger number of electrostatic contacts of opposite signs and thus increases particle adsorption onto PMAA brushes. Further increase in pH reduces the number of positive charges on the particles and concurrently leads to a stronger charging within the brush, which results in a slight decrease in the particle density. While all these trends are confirmed in the data shown in Figure 10, we see additionally that there is a relatively large population of PS-NH<sub>2</sub> particles adsorbing on PMAA brushes at high pH. We attribute this behavior to hydrogen bonding between the particles and the PMAA segments. The partitioning of functionalized PS particles on PDMAEMA and PMAA brushes will serve as a benchmark in interpreting particle adsorption on polyampholyte brush surfaces (cf. Figure 11).

The adsorption of functionalized PS beads on polyampholyte brushes is more complex than that on homopolymer brushes. At low pH the PDMAEMA block is fully charged while there are only a few charges present for the PMAA block. Due to repulsion between positive charges along the PDMAEMA block, the block copolymer extends into the solution. A complementary situation takes place at high pH values, where the PMAA block is charged and extended due to electrostatic repulsion acting between negative charges, while the PDMAEMA block possesses only a few charges. On the basis of the data in Figure 11, at low and high pH values, far away from the pK<sub>a</sub> of amines and carboxylic acids on PS particles, PMAA, and PDMAEMA, adsorption of both functionalized particles resembles closely their behavior on homopolymer brushes. This indicates that at extreme values of pH particle adsorption is governed primarily by the characteristics of the top block of the polyampholyte copolymer brush.

Up to this point we only invoked enthalpic interactions to explain partitioning of functionalized PS particles on weak polyelectrolyte brushes. This is clearly an oversimplification because in addition to enthalpy particle adsorption will depend on conformational changes of polymers associated with not only the presence of charges but also the density of polymers on the surface and the sizes of the particles relative to those of the brush. In particular, considering that the grafting density of brushes is relatively large (typically 0.4–0.5 nm<sup>-2</sup> for these type of polymerizations<sup>75</sup>) and the brushes are much smaller than the particles, it is reasonable to consider that the penetration of particles inside the brushes is rather small.<sup>76,77</sup> Therefore, the particles interact with those segments of the brush that are close to the brush periphery. These considerations will be important when explaining the adsorption of PS particles onto polyampholytic brushes in solutions having pH between 4 and 8. Due to both positive and negative charges present in PDMAEMA and PMAA in this pH range, the brushes may form compact/collapsed structures,<sup>19</sup> with individual chains interacting, collapsing on themselves, or collapsing on their neighbors (cf. Figures 1 and 9). Due to those conformational (and morphological) changes in the brush structure (portions of) both the top and the bottom blocks are present close to the tip of the brush (cf. Figure 1) and may interact with the particle. This behavior is most pronounced in the adsorption of PS-NH<sub>2</sub> on SiO<sub>x</sub>/PMAA-*b*-PDMAEMA (second row in Figure 11) and that of PS-COOH on SiO<sub>x</sub>/PDMAEMA-*b*-PMAA (third row in Figure 11). While the amount of PS-NH<sub>2</sub> adsorbing on SiO<sub>x</sub>/PDMAEMA is low at all pH values studied, there is a considerable increase in the

concentration of PS-NH<sub>2</sub> particles in SiO<sub>x</sub>/PDMAEMA-*b*-PMAA at pH 5.5 and 10. We attribute this behavior largely to electrostatic interactions between the PS-NH<sub>2</sub> particles and the bottom PMAA brush that is exposed due to a partial collapse of the PMAA and PDMAEMA blocks. Similar behavior can be observed when considering the adsorption of PS-COOH particles on top of SiO<sub>x</sub>/PDMAEMA-*b*-PMAA. An increase in particle uptake in this system relative to that observed in PMAA homopolymer is attributed to interactions between negatively charged carboxylate groups in the particle and positively charged units in the bottom PDMAEMA brush. We appreciate that these conclusions may appear to be at odds with the WCA experiments that did not exhibit any anomalies as a function of pH. We note that more comprehensive experiments, some of them suggested in the Conclusions section, will have to be carried out in order to gain a more comprehensive understanding of the structure of polyampholytic brushes and their conformational variation in response to environmental changes involving pH, salt concentration, and other factors.

#### 4. CONCLUSIONS

Ampholytic block copolymer brushes were prepared by “surface-initiated” sequential polymerization of NaMA and DMAEMA by following the ARGET-ATRP protocol followed by subsequent conversion of PNaMA to PMAA. We followed the kinetics of ARGET-ATRP of NaMA on surfaces by combined UV-vis and ellipsometric studies for various AA/CuCl<sub>2</sub> ratios. Conversion of PNaMA to PMAA was confirmed by XPS. Utilization of ARGET-ATRP to produce PNaMA and ultimately PMAA is the major difference to previous reports that have employed ATRP to generate PtBMA that acted as a precursor to PMAA. ARGET-ATRP reaction is faster than conventional ATRP; thus, thicker brushes can be grown at room temperature in aqueous solvents utilizing a lower concentration of copper catalyst. Another advantage of using PNaMA is that protonation that yields PMAA proceeds under mild reaction conditions, thus avoiding any degradation of the grafted macromolecules. We demonstrated the ability to polymerize DMAEMA from PNaMA macroinitiators as well as growth of PNaMA from PDMAEMA macroinitiators. Those reactions led to formation of polyampholytic brushes on silica surfaces, i.e., SiO<sub>x</sub>/PNaMA-*b*-PDMAEMA and SiO<sub>x</sub>/PDMAEMA-*b*-PNaMA. The changes in the dry thickness of PNaMA brushes elucidated from ellipsometry measurements confirm that conversion of PNaMA blocks in polyampholytes does not degrade the PDMAEMA block. Because both polymerizations proceed under virtually the same reaction conditions, one can broaden the repertoire of monomer sequences from diblock to random copolymers. This may be interesting as the comonomer sequence distribution in polyampholytes is expected to lead to large conformational changes of such brushes.

We examined the response of polyampholytic block copolymer brushes to variation of pH. Contact angle experiments using aqueous solutions with variable pH revealed that the copolymer brush response was identical to that of a homopolymer whose chemical composition was identical to the top block of the polyampholytic brush. In order to provide evidence that ampholytic diblock copolymers are indeed formed, we use them as substrates for adsorption of polystyrene latex spheres with two different functionalities, i.e., amine- and carboxy-terminated. Although not quantitative, overall the particle adsorption experiments provide

clear evidence that conformations in ampholytic diblock copolymer brushes are different than those in homopolymers. More work needs to be done, however, to provide a more comprehensive and quantitative description of polyampholyte behavior at interfaces. In particular, polyampholytic diblocks with lower grafting densities than those employed in this study should be used; such systems should exhibit larger conformational changes of the grafts due to greater free volume.

## ■ AUTHOR INFORMATION

### Corresponding Author

\*E-mail: Jan\_Genzer@ncsu.edu.

### Present Addresses

<sup>§</sup>Intel Corporation, Portland, Oregon 97124, United States.

<sup>¶</sup>University of California at Berkeley, Berkeley, California 94720, United States.

## ■ ACKNOWLEDGMENT

This work was funded in part by the National Science Foundation and the Army Research Office. Y.K.J. thanks the National Research Council Research Associateship Award Program at the Army Research Office. The authors thank Ms. Elizabeth Melvin and Prof. Orlin Velev for their assistance with fluorescence microscopy measurements.

## ■ REFERENCES

- (1) Park, J. W.; Thomas, E. L. *J. Am. Chem. Soc.* **2002**, *124* (4), 514.
- (2) Zhao, B.; Brittain, W. J. *Prog. Polym. Sci.* **2000**, *25* (5), 677.
- (3) Chen, M.; Briscoe, W. H.; Armes, S. P.; Klein, J. *Science* **2009**, *323* (5922), 1698.
- (4) Li, D. J.; Sheng, X.; Zhao, B. *J. Am. Chem. Soc.* **2005**, *127* (17), 6248.
- (5) Prime, K. L.; Whitesides, G. M. *J. Am. Chem. Soc.* **1993**, *115* (23), 10714.
- (6) Israels, R.; Leermakers, F. A. M.; Fleer, G. J. *Macromolecules* **1995**, *28* (5), 1626.
- (7) Arifuzzaman, S.; Özçam, A. E.; Efimenko, K.; Fischer, D. A.; Genzer, J. *Biointerphases* **2009**, *4* (2), FA33.
- (8) Cohen Stuart, M.; Huck, W.; Genzer, J.; Müller, M.; Ober, C. K.; Stamm, M.; Sukhorukov, G.; Szleifer, I.; Tsukruk, V.; Urban, M.; Winnik, F.; Zauscher, S.; Luzinov, I.; Minko, S. *Nat. Mater.* **2010**, *9*, 101.
- (9) Galvin, C. J.; Genzer, J. *Prog. Polym. Sci.* **2011**, in press; DOI: 10.1016/j.progpolymsci.2011.12.001.
- (10) Brittain, W. J.; Ayres, N.; Boyes, S. G. *Langmuir* **2007**, *23* (1), 182.
- (11) Brittain, W. J.; Ayres, N.; Cyrus, C. D. *Langmuir* **2007**, *23* (7), 3744.
- (12) Sanjuan, S.; Perrin, P.; Pantoustier, N.; Tran, Y. *Langmuir* **2007**, *23* (10), 5769.
- (13) Tran, Y.; Sanjuan, S. *Macromolecules* **2008**, *41* (22), 8721.
- (14) Tran, Y.; Combellas, C.; Kanoufi, F.; Sanjuan, S.; Slim, C. *Langmuir* **2009**, *25* (9), 5360.
- (15) Han, Y. C.; Yu, K. *Soft Matter* **2009**, *5* (4), 759.
- (16) Bhat, R. R.; Tomlinson, M. R.; Wu, T.; Genzer, J. *Adv. Polym. Sci.* **2006**, *198*, 51.
- (17) Dautzenberg, H.; Jaeger, W.; Kotz, J.; Philipp, B.; Seidel, C.; Stscherbina, D. *Polyelectrolytes: Formation, Characterization and Application*; Hanser Publishers: Munich, 1994.
- (18) Everaers, R.; Johner, A.; Joanny, J. F. *Europhys. Lett.* **1997**, *37* (4), 275.
- (19) Harada, A.; Kataoka, K. *Science* **1999**, *283* (5398), 65.
- (20) Ayres, N.; Cyrus, C. D.; Brittain, W. J. *Langmuir* **2007**, *23* (7), 3744.
- (21) Hinrichs, K.; Aulich, D.; Ionov, L.; Esser, N.; Eichhorn, K.-J.; Motornov, M.; Stamm, M.; Minko, S. *Langmuir* **2009**, *25* (18), 10987.
- (22) Osborne, V. L.; Jones, D. M.; Huck, W. T. S. *Chem. Commun.* **2002**, *17*, 1838.
- (23) Sanjuan, S.; Tran, Y. *Macromolecules* **2008**, *41* (22), 8721.
- (24) Yu, K.; Wang, H.; Xue, L.; Han, Y. *Langmuir* **2006**, *23* (3), 1443.
- (25) Brandrup, J.; Immergut, E. H.; Grulke, E. A. *Polymer Handbook*, 4th ed.; Wiley & Sons: New York, 1999.
- (26) Ando, T.; Kato, M.; Kamigaito, M.; Sawamoto, M. *Macromolecules* **1996**, *29* (3), 1070.
- (27) Matyjaszewski, K.; Patten, T. E.; Xia, J. *J. Am. Chem. Soc.* **1997**, *119* (4), 674.
- (28) Patten, T. E.; Matyjaszewski, K. *Adv. Mater.* **1998**, *10* (12), 901.
- (29) Sankhe, A. Y.; Husson, S. M.; Kilbey, S. M. *Macromolecules* **2006**, *39* (4), 1376.
- (30) Mykytiuk, J.; Armes, S. P.; Billingham, N. C. *Polym. Bull.* **1992**, *29* (1–2), 139.
- (31) Rannard, S. P.; Billingham, N. C.; Armes, S. P.; Mykytiuk, J. *Eur. Polym. J.* **1993**, *29* (2–3), 407.
- (32) Boyes, S. G.; Akgun, B.; Brittain, W. J.; Foster, M. D. *Macromolecules* **2003**, *36* (25), 9539.
- (33) Haddleton, D. M.; Crossman, M. C.; Dana, B. H.; Duncalf, D. J.; Heming, A. M.; Kukulj, D.; Shooter, A. J. *Macromolecules* **1999**, *32* (7), 2110.
- (34) Kurosawa, S.; Aizawa, H.; Talib, Z. A.; Atthoff, B.; Hilborn, J. *Biosens. Bioelectron.* **2004**, *20* (6), 1165.
- (35) Matyjaszewski, K.; Miller, P. J.; Shukla, N.; Immaraporn, B.; Gelman, A.; Luokala, B. B.; Siclovan, T. M.; Kickelbick, G.; Vallant, T.; Hoffmann, H.; Pakula, T. *Macromolecules* **1999**, *32* (26), 8716.
- (36) Sanjuan, S.; Tran, Y. *J. Polym. Sci., Part A: Polym. Chem.* **2008**, *46* (13), 4305.
- (37) Treat, N. D.; Ayres, N.; Boyes, S. G.; Brittain, W. J. *Macromolecules* **2005**, *39* (1), 26.
- (38) Wu, T. G., J.; Gong, P.; Szleifer, I.; Vlcek, P.; Šubr, V. In *Polymer Brushes: Synthesis, Characterization, Applications*; Advincula, R. C., Brittain, W. J., Caster, K. C., Rühe, J., Eds.; Wiley: Weinheim, 2004.
- (39) Ashford, E. J.; Naldi, V.; O'Dell, R.; Billingham, N. C.; Armes, S. P. *Chem. Commun.* **1999**, *14*, 1285.
- (40) Tugulu, S.; Barbey, R.; Harms, M.; Fricke, M.; Volkmer, D.; Rossi, A.; Klok, H.-A. *Macromolecules* **2006**, *40* (2), 168.
- (41) Dong, R.; Krishnan, S.; Baird, B. A.; Lindau, M.; Ober, C. K. *Biomacromolecules* **2007**, *8* (10), 3082.
- (42) Dong, R.; Lindau, M.; Ober, C. K. *Langmuir* **2009**, *25* (8), 4774.
- (43) Shen, Y.; Tang, H.; Ding, S. *Prog. Polym. Sci.* **2004**, *29* (10), 1053.
- (44) Haddleton, D. M.; Kukulj, D.; Radigue, A. P. *Chem. Commun.* **1999**, *1*, 99.
- (45) Hong, S. C.; Matyjaszewski, K. *Macromolecules* **2002**, *35* (20), 7592.
- (46) Kickelbick, G.; Paik, H.-j.; Matyjaszewski, K. *Macromolecules* **1999**, *32* (9), 2941.
- (47) Kubisa, P. *Prog. Polym. Sci.* **2004**, *29* (1), 3.
- (48) Matyjaszewski, K.; Pintauer, T.; Gaynor, S. *Macromolecules* **2000**, *33* (4), 1476.
- (49) Qiu, J.; Charleux, B.; Matyjaszewski, K. *Prog. Polym. Sci.* **2001**, *26* (10), 2083.
- (50) Sarbu, T.; Matyjaszewski, K. *Macromol. Chem. Phys.* **2001**, *202* (17), 3379.
- (51) Jakubowski, W.; Min, K.; Matyjaszewski, K. *Macromolecules* **2006**, *39* (1), 39.
- (52) Jakubowski, W.; Matyjaszewski, K. *Angew. Chem., Int. Ed.* **2006**, *45* (27), 4482.
- (53) Matyjaszewski, K.; Jakubowski, W.; Min, K.; Tang, W.; Huang, J. Y.; Braunecker, W. A.; Tsarevsky, N. V. *Proc. Natl. Acad. Sci. U.S.A.* **2006**, *103* (42), 15309.
- (54) Tomlinson, M. R.; Genzer, J. *Polymer* **2008**, *49*, 4837.

- (55) Tugulu, S.; Barbey, R.; Harms, M.; Fricke, M.; Volkmer, D.; Rossi, A.; Klok, H. A. *Macromolecules* **2007**, *40* (2), 168.
- (56) Mori, H.; Muller, A. H. E. *Prog. Polym. Sci.* **2003**, *28* (10), 1403.
- (57) Sukhishvili, S. A.; Granick, S. *Macromolecules* **2002**, *35* (1), 301.
- (58) Matyjaszewski, K.; Dong, H.; Jakubowski, W.; Pietrasik, J.; Kusumo, A. *Langmuir* **2007**, *23* (8), 4528.
- (59) Berends, H. P.; Stephan, D. W. *Inorg. Chem.* **1987**, *26* (5), 749.
- (60) Breeze, S. R.; Wang, S. *Inorg. Chem.* **1996**, *35* (11), 3404.
- (61) Osako, T.; Karlin, K. D.; Itoh, S. *Inorg. Chem.* **2005**, *44* (2), 410.
- (62) Tomlinson, M. R.; Efimenko, K.; Genzer, J. *Macromolecules* **2006**, *39* (26), 9049.
- (63) Ozcam, A. E.; Efimenko, K.; Jaye, C.; Spontak, R. J.; Fischer, D. A.; Genzer, J. *J. Electr. Spectrosc. Relat. Phenom.* **2009**, *172*, 95.
- (64) Windawi, H.; Ho, F. F. *Applied Electron Spectroscopy for Chemical Analysis*; Wiley: New York, 1982.
- (65) Briggs, D. J. *Surface Analysis of Polymers by XPS and Static SIMS*; Cambridge University Press: Cambridge, U.K., 1998.
- (66) Davidson, R. L. *Handbook of water-soluble gums and resins*; McGraw-Hill: New York, 1980.
- (67) van de Wetering, P.; Zuidam, N. J.; van Steenbergen, M. J.; van der Houwen, O. A. G. J.; Underberg, W. J. M.; Hennink, W. E. *Macromolecules* **1998**, *31* (23), 8063.
- (68) Gong, P.; Wu, T.; Genzer, J.; Szleifer, I. *Macromolecules* **2007**, *40* (24), 8765.
- (69) Zhu, T.; Fu, X. Y.; Mu, T.; Wang, J.; Liu, Z. F. *Langmuir* **1999**, *15* (16), 5197.
- (70) Genzer, J.; Bhat, R. R.; Fischer, D. A. *Langmuir* **2002**, *18* (15), 5640.
- (71) Rubner, M. F.; Yoo, D.; Shiratori, S. S. *Macromolecules* **1998**, *31* (13), 4309.
- (72) Rubner, M. F.; Shiratori, S. S. *Macromolecules* **2000**, *33* (11), 4213.
- (73) Wei, S.; Tzeng, W. B.; Castleman, A. W. *J. Phys. Chem.* **1990**, *94* (18), 6927.
- (74) Aviyente, V.; Varnali, T. *Theochem. J. Mol. Struct.* **1994**, *118* (1), 85.
- (75) Tomlinson, M. R.; Genzer, J. *Langmuir* **2005**, *21* (25), 11552.
- (76) Bhat, R. R.; Genzer, J. *Nanotechnology* **2007**, *18*, 025301.
- (77) Bhat, R. R.; Genzer, J. *Appl. Surf. Sci.* **2005**, *252*, 2549.